Does the MJO Have a Westward Group Velocity?

GUOSEN CHEN

Earth System Modeling Center, Nanjing University of Information Science and Technology, Nanjing, China, and Department of Atmospheric Sciences and Atmosphere–Ocean Research Center, University of Hawai'i at Mānoa, Honolulu, Hawaii

BIN WANG

Department of Atmospheric Sciences and Atmosphere–Ocean Research Center, University of Hawai'i at Mānoa, Honolulu, Hawaii, and Earth System Modeling Center, Nanjing University of Information Science and Technology, Nanjing, China

(Manuscript received 7 July 2017, in final form 30 December 2017)

ABSTRACT

Current theoretical studies have a debate on whether the Madden–Julian oscillation (MJO) has a zero or westward group velocity. A recent analysis of the observed Hovmöller diagram of MJO signals suggested that the MJO has a significant westward group velocity. Here it is shown that the observed MJO has a negligibly small group velocity, which is manifested in two aspects. First, on the wavenumber–frequency spectra diagram the precipitation spectra indicate quasi independence of the MJO frequency on wavenumber, suggesting a nearly vanishing group velocity. Second, on the Hovmöller diagram of the regressed intraseasonal daily precipitation, the MJO group velocity is defined by the propagation of the wave envelopes of the precipitation and is shown to be negligibly small for the eastward propagating signals. The causes of the discrepancy between this study and the recent study mentioned above are the calculating method and the data filtering process. The group velocity in the recent study is calculated by the propagation of local convection extrema, which does not necessarily indicate the propagation of the wave envelopes. More importantly, the westward propagation of the local convection extrema is an artifact of the data filtering. The Hovmöller diagram in the recent study was constructed by using only the eastward propagating wavenumber-1–5 signals. This truncation of data onto the planetary scales of the eastward wavenumber domain fails to resolve the Maritime Continent ''barrier effect,'' causing significant artificial westward propagation of local convection extrema.

1. Introduction

The Madden–Julian oscillation (MJO) (Madden and Julian 1971, 1972) is a low-frequency (30–90 days), convectively coupled planetary-scale system that propagates slowly eastward with a speed of about 3–6 m s^{-1} from the Indian Ocean (IO) to the western Pacific (WP) (Knutson et al. 1986; Zhang and Ling 2017). The MJO is the dominant component of the tropical intraseasonal variability and the eastward propagation of the MJO is manifested in both the dynamic and the convective fields (Zhang 2005), such as 850-hPa zonal wind and precipitation. The MJO has a distinctive dispersion relation that differs from other theoretical equatorial waves on the wavenumber–frequency spectra diagram (Wheeler and Kiladis 1999; Hendon and Wheeler 2008). Analogous to the linear equatorial wave theory, we can define the phase propagation velocity and the group velocity for the MJO. The phase velocity of the MJO indicates the phase propagation of the MJO, while the group velocity of the MJO indicates the energy dispersion of the MJO. Since the MJO plays a crucial role in bridging weather and climate (Zhang 2013), it is important to understand both its phase propagation and energy dispersion features.

Although the eastward phase propagation of the MJO and the associated mechanisms have been extensively studied, the dispersion relation of the MJO and the associated group velocity feature have been less emphasized. Previously, the observational evidences indicated that the MJO's frequency is quasi constant with respect to wavenumber on the wavenumber–frequency spectra diagram (Salby et al. 1994; Wheeler and Kiladis 1999;

Corresponding author: Guosen Chen, chenguos@hawaii.edu

DOI: 10.1175/JCLI-D-17-0446.1

Roundy and Frank 2004; Hendon and Wheeler 2008; Jiang et al. 2015), implying a vanishing group velocity for the MJO. This quasi-constant frequency feature was also considered to be a target for theoretical modeling of the MJO (Majda and Stechmann 2009), and this peculiar dispersion feature has been reproduced in some linear theoretical models (Majda and Stechmann 2009; Liu and Wang 2012, 2017a,b). Recently, on the other hand, Adames and Kim (2016, hereafter AK16) showed that the MJO is a dispersive convectively coupled moisture wave, which has a significant westward group velocity. They showed that the westward group velocity has a magnitude of about 40% as large as its phase speed. Their results contrast with previous view that the MJO has a near-zero group velocity.

The major observational support of AK16's argument is the Hovmöller diagram of the MJO propagation. The authors decomposed the data into eastward and westward propagating wave signals, and they showed a westward propagation of the local convection extrema (the maximum or minimum convection centers on the Hovmöller diagram) for the filtered eastward propagating wavenumber-1–5 signals. They then calculated the group velocity of the MJO in terms of this propagation of local extrema and concluded that the MJO has a significant westward group velocity. However, in reality, the group velocity is represented by the propagation of wave envelopes. The locations of local convection extrema do not necessarily indicate the locations of maximum wave envelopes. Thus, it is questionable whether the propagation of local extrema is equivalent to the propagation of wave envelopes and whether the MJO has a westward group velocity. Another issue is that the Hovmöller diagram for the total intraseasonal convective signals (including both the eastward and the westward propagating wave signals) shows nonpropagation of local convection extrema in many other studies (e.g., Jiang et al. 2015; Chen and Wang 2017; Liu and Wang 2017b; Wang et al. 2017; Wang and Lee 2017). Thus, it is also questionable whether the westward propagation of local convection extrema is caused by the data filtering process.

Understanding whether the MJO has a westward group velocity has important implications for intraseasonal weather prediction. Analogous to midlatitude Rossby waves, if the MJO has a westward group velocity, then the energy of the MJO will disperse ''upstream'' (relative to the direction of its phase propagation). That is, the development of the MJO over the WP region will affect the MJO initiation over the IO region. In this study, we reexamine the observed group velocity and dispersion relation of the MJO to see whether the MJO has a westward group velocity. The data and methodology are described in section 2. The observed dispersion relation and propagation features of the MJO are shown in section 3. Different methods have been used to estimate the group velocity of the MJO. In section 4, the causes of the discrepancy in calculating the MJO group velocity are investigated. The conclusions and a discussion are given in section 5.

2. Data and methodology

The datasets used in this study include the high horizontal resolution (0.25° × 0.25°) eight times daily precipitation rate ($mm\,h^{-1}$) and the daily accumulated precipitation (mm) from the 3B42, version 7, product of the Tropical Rainfall Measuring Mission (TRMM-3B42) (Huffman et al. 2007), based on the period of record from 1998 to 2016. To eliminate small-scale noises and reduce computation time, the high horizontal resolution TRMM dataset is interpolated into lower horizontal resolution (1° × 1°). In this study, we focus on the northern winter from November to April (NDJFMA).

The methods used in this study include the wavenumber–frequency spectra analysis, the data filtering, and the wave envelope calculation. To reveal the dispersion relation of MJO convection signals, the wavenumber–frequency spectra of the eight times daily precipitation rate are calculated by using the method of Wheeler and Kiladis (1999). First, the seasonal cycle has been removed. Then for each year, we use a 182-day (which covers NDJFMA) nonoverlapping window to calculate the power spectra. The method of Hayashi (1971) is used to resolve the power spectra into progressive (eastward) and retrogressive (westward) wave components. To get smooth spectra, a 1–2–1 filter has been applied to the calculated raw spectra on the frequency dimension. Using the unsmoothed raw spectra will lead to the same conclusions.

To produce the Hovmöller diagram for the MJO propagation, the data filtering is applied to the daily precipitation data. The data filtering processes include temporal filtering and wavenumber filtering. To extract intraseasonal signals, a 20–100-day Lanczos filter (Duchon 1979) is applied to the daily accumulated precipitation data. To further decompose the intraseasonal signals on the Hovmöller diagram into eastward and westward propagating wave signals, a 2D Fourier analysis is applied to the longitude and time dimensions.

To study the group velocity of the MJO, the wave envelopes of the MJO convection are calculated by using the method provided by Hayashi (1982). Following Hayashi (1982), the wave packets with wavenumber band Δk can be expressed as

$$W_{\Delta k}(x,t) = \mathrm{Re}\sum_{\Delta k} W_k(t)e^{ikx} = \mathrm{Re}\,\alpha(x,t)e^{i\phi(x,t)}, \quad (1)$$

where α and ϕ are envelope and phase of the wave packets. The envelope α can be expressed as

$$\alpha = \left|\sum_{\Delta k} W_k(t)e^{ikx}\right| = (c^2 + s^2)^{1/2}, \quad (2)$$

where c and s are the real and imaginary parts of the complex Fourier series and are defined as

$$c(x,t) = \sum_{\Delta k}[C_k(t)\cos(kx) + S_k(t)\sin(kx)] \quad (3)$$

and

$$s(x,t) = \sum_{\Delta k}[-C_k(t)\sin(kx) + S_k(t)\cos(kx)], \quad (4)$$

where $C_k(t)$ and $S_k(t)$ are the cosine and sine coefficients.

Figure 1 shows an example of the wave packets of MJO convection signals and their associated wave envelopes. The black solid curves indicate the carrier wave packets, while the blue dashed curves indicate the associated wave envelopes, which are smooth curves outlining the amplitudes of the oscillating wave packets. The black dashed line illustrates the longitude variations of the carrier wave crest with time, which indicates the phase propagation of the carrier wave packets; the black solid line illustrates the longitude variations of the maximum wave envelope with time, which indicates the propagation of the wave envelopes. As illustrated in Fig. 1, the wave crests propagate eastward systematically (phase propagation; dashed line), while the wave envelopes almost do not propagate with time (energy dispersion; solid line).

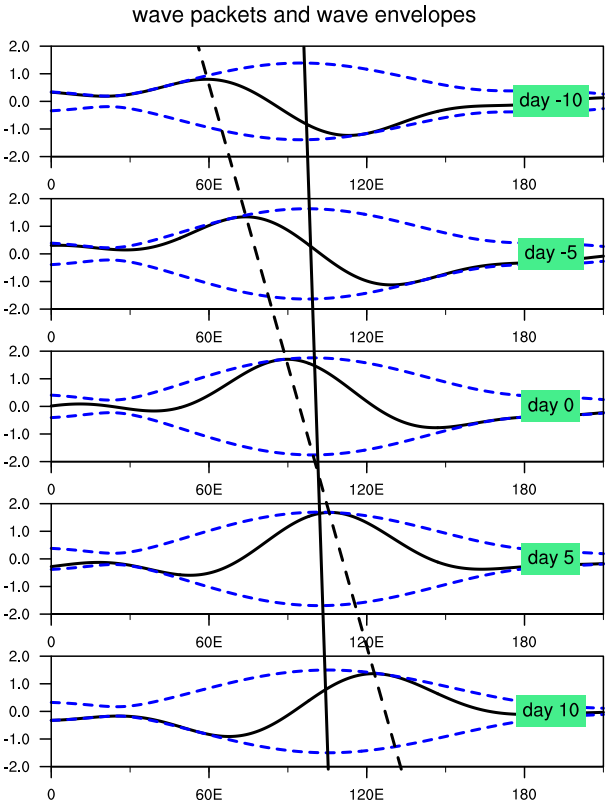

FIG. 1. Illustration of wave packets and the associated wave envelopes: the time-lagged evolution of wave packets (black solid curves) and their corresponding wave envelopes (blue dashed curves). The wave packets are obtained by first regressing the intraseasonal daily precipitation anomalies against themselves averaged over the equatorial eastern Indian Ocean (10°S–10°N, 75°–100°E). The regression is performed with lags from −50 days to +50 days with 1-day interval. Then the lag-regressed signals are further filtered into the eastward propagating wavenumber-1–5 signals. The wave envelopes are then calculated by using Eq. (2). The solid line illustrates the propagation of wave envelope and the dashed line illustrates the propagation of the wave crest.

3. Observed dispersion relation and group velocity of the MJO

To study the general dispersion features of the MJO, the wavenumber–frequency power spectra of the symmetric component of the eight times daily precipitation rate during the northern winter (NDJFMA) are shown in Fig. 2. It shows the raw power spectra summed over 10°S–10°N. As shown in Fig. 2, the MJO convection signals concentrate on the planetary scales (wavenumbers 1–5) of the eastward propagating wavenumber domain. The blue circles mark the locations of the centroid frequency in the MJO band (30–90 days) for eastward wavenumbers 1–5. The centroid frequency for each wavenumber is calculated as $f_c = \int_{1/90d}^{1/30d} fS(f)\,df / \int_{1/90d}^{1/30d} f\,df$, where f_c is the centroid frequency, f is the frequency, and S is the spectrum. The thick solid line is a linear least squares fit of the centroid frequencies. This least squares fit line shows the approximate dispersion relation of the MJO, which indicates that the MJO has a quasi-constant frequency with respect to wavenumber. This is consistent with previous studies (Salby et al. 1994; Wheeler and Kiladis 1999; Roundy and Frank 2004; Hendon and Wheeler 2008; Jiang et al. 2015). The group velocity estimated from the linear least squares fit line shows a vanishing group speed ($C_g = \partial\omega/\partial k \approx 0$ m s^{-1}). In summary, the wavenumber–frequency spectra analysis indicates that the MJO has a quasi-constant frequency and a consequent near-zero group velocity.

The propagation features of the MJO can be further examined by the Hovmöller diagram. Figure 3 shows the Hovmöller diagram of the daily precipitation anomalies

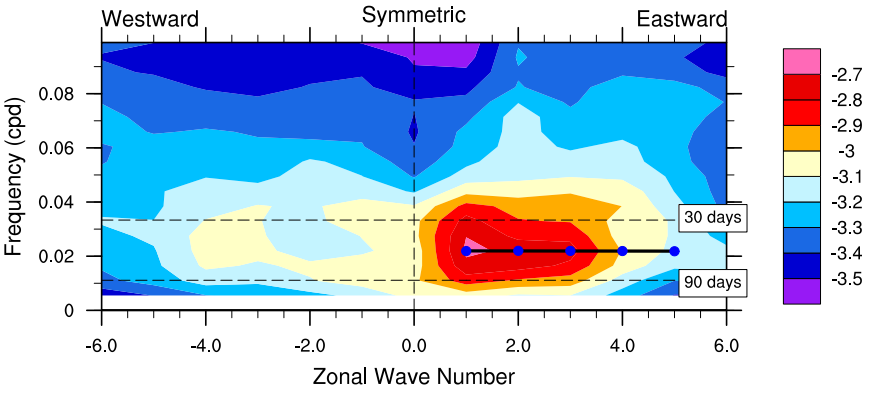

FIG. 2. Wavenumber–frequency power spectra of the symmetric component of the TRMM eight times daily precipitation rate, plotted as the raw spectra power summed over 10°S–10°N. The logarithm (base 10) has been applied to the spectra for plotting. The blue circles mark the centroid frequencies in the intraseasonal band for wavenumbers 1–5. The black solid line, which shows the approximate dispersion relation of the MJO, is the linear least squares fit of the centroid frequencies.

(mm; shadings) over the tropics (10°S–10°N) based on the lag regression of the intraseasonal daily accumulated precipitation against themselves averaged over the IO (10°S–10°N, 75°–100°E), the Maritime Continent (MC; 10°S–10°N, 110°–135°E), and the WP (10°S–10°N, 135°–160°E). It is shown by Fig. 3 that the precipitation anomalies propagate eastward systematically in all three panels. This reflects the propagation features of the MJO. The results here show consensus with previous studies (Jiang et al. 2015; Chen and Wang 2017; Wang and Lee 2017). The MJO convection starts from the IO and dissipates near the date line, as shown in all panels of Fig. 3. It also shows that the MJO convection signal is weakened as it approaches the MC region. This

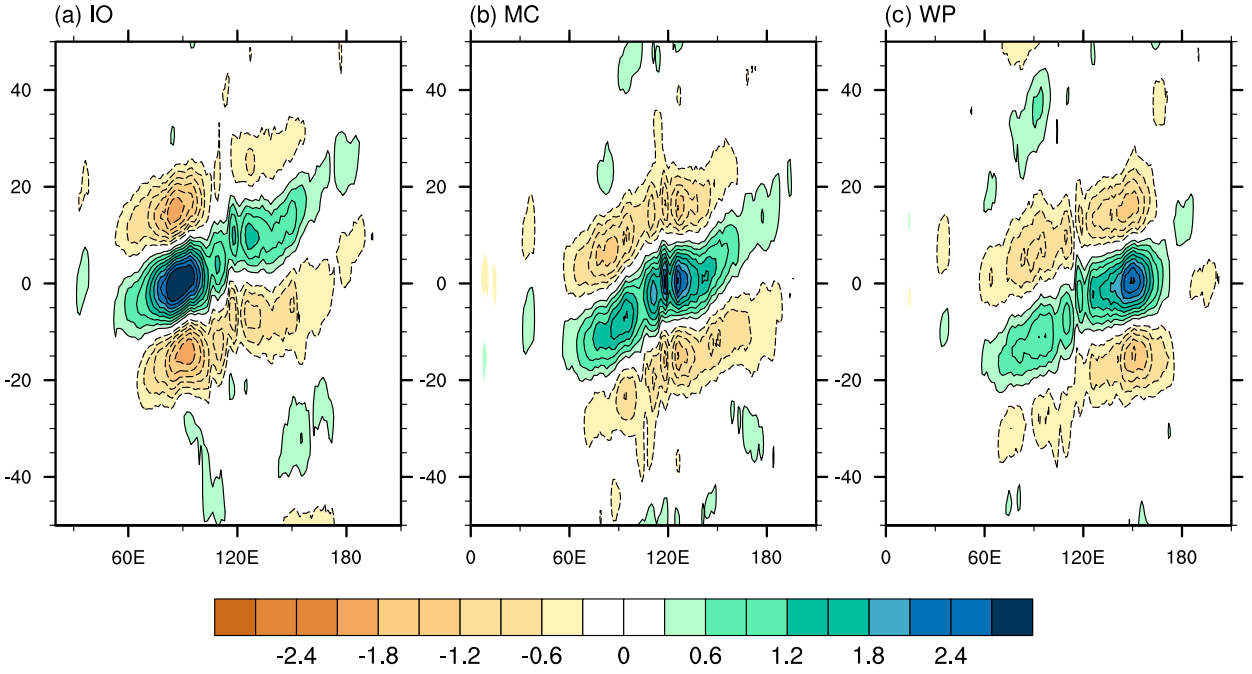

FIG. 3. Longitude–time evolution of the intraseasonal daily precipitation anomalies (mm; shadings) over the tropics (10°S–10°N) by lag regression (with 1-day interval) of intraseasonal daily precipitation anomalies against themselves averaged over (a) the equatorial Indian Ocean (10°S–10°N, 75°–100°E), (b) the equatorial Maritime Continent (10°S–10°N, 110°–135°E), and (c) the equatorial western Pacific (10°S–10°N, 135°–160°E). Only those above the 90% confidence level are shaded.

weakening of MJO signal over the MC is due to the so-called MC barrier effect (Rui and Wang 1990; Zhang and Ling 2017). This MC barrier effect is manifested in all three panels of Fig. 3.

Physically, the group velocity represents the propagation speed of wave envelopes. To examine the propagation of the MJO wave envelopes and to compare it with the wavenumber–frequency spectra diagram, we first decompose the MJO convection signals in Fig. 3 into eastward and westward propagating wave signals by using a 2D Fourier analysis. The color shadings in the upper panels of Fig. 4 show the total eastward propagating wave signals corresponding to Fig. 3. The associated wave envelopes are then calculated by using Eq. (2). The contours in Fig. 4 depict the corresponding longitude–time evolution of the wave envelopes. To depict the propagation speed of the wave envelope, we calculate the centroid longitude of the wave envelope at each time step from day −30 to day 30. The centroid longitude of the wave envelope over the Indo-Pacific sector (45°E–180°) is calculated as $x_c = \int_{45E}^{180} xA(x)\,dx / \int_{45E}^{180} xdx$, where x_c is the centroid longitude, x is the longitude, and $A(x)$ is the wave envelope. The black solid lines in Fig. 4 show the linear least squares fit of the centroid longitudes. It shows that the wave envelopes of MJO signals exhibit a nearly nonpropagating feature. If we define the group velocity C_g as the propagation speed of the centroid longitude of the wave envelope, then the calculated C_g is eastward and on the order of $+0.2\,\mathrm{m\,s^{-1}}$, which is negligibly small compared to the phase speeds [$C_p \sim O(+4)\,\mathrm{m\,s^{-1}}$, shown in Fig. 4]. Since the MJO signals concentrate on planetary scales, the lower panels of Fig. 4 further show the filtered eastward propagating wavenumber-1–5 signals. It shows that the group velocities for the eastward propagating wavenumber-1–5 signals are basically identical to those of the total eastward propagating wave signals. In summary, Fig. 4 indicates that the MJO has a negligible small group velocity, which is roughly consistent with the result of the wavenumber–frequency spectra analysis (Fig. 2).

4. The causes of the discrepancy in calculating the group velocity

The group velocities of the MJO are found to be negligibly small in Figs. 2 and 4, which contrasts with the results of AK16. The authors of AK16 calculated the group velocity in terms of the propagation of local convection extrema on the Hovmöller diagram. This method stems from the original purpose of the Hovmöller diagram (Persson 2017) that sought to understand the dispersion features of the midlatitude Rossby waves. As shown in the lower panels of Fig. 4, the local convection extrema (marked by red crosses) show significant westward propagations. Let us define C_e as the propagation speed of the local convection extrema. The calculated C_e for the eastward propagating wavenumber-1–5 signals is westward and has the order of $-2.5\,\mathrm{m\,s^{-1}}$, which is consistent with AK16. Since C_g has the order of $+0.2\,\mathrm{m\,s^{-1}}$, it shows that the two methods produce quite different results for the eastward propagating wavenumber-1–5 signals.

One of the reasons why the two methods produce such different results is that the propagation of local wave extrema does not necessarily indicate the propagation of wave envelopes. As illustrated in Fig. 1, the maximum wave envelope does not necessarily coincide with the phase extremum of the carrier wave packets. Thus, the propagation of local wave extrema is not equivalent to the propagation of wave envelopes. As illustrated in lower panels of Fig. 4, the wave envelopes of the MJO convection almost do not propagate (black solid lines) while the local convection extrema propagate westward (brown solid lines). Given the fact that the calculated C_g values by the wave envelopes show consensus with the value estimated by the wavenumber–frequency spectra diagram, and that the group velocity is interpreted as the propagation speed of wave envelopes, it indicates that using C_g to estimate the group velocity of the MJO is more robust and reasonable than using C_e.

Another reason why the two methods produce such different results is related to the data filtering process. As shown in Figs. 3a–c, there is no obvious westward propagation of the local convection extrema in the total intraseasonal signals. For example, the local convection extrema in Fig. 3a over the IO and the WP stay in the IO and the WP, which indicates stationary propagations of the local convection extrema. The same is true for Figs. 3b and 3c. Thus, this raises a question: is the westward propagation of the local extrema an artifact of the data filtering process?

To answer this question, Fig. 5 compares the total intraseasonal signals [first column (identical to Fig. 3)], the total intraseasonal eastward propagating wave signals (second column), the intraseasonal eastward propagating wavenumber-1–5 signals (third column), and the total (eastward + westward) intraseasonal wavenumber-1–5 signals (fourth column). Compared to the total signals (first column), the MC barrier effect in the total eastward propagating wave signals (second column) is less significant. This is because the MC barrier effect can spread the MJO signals into strong eastward propagating wave signals and weak westward propagating wave signals (Zhang and Hendon 1997). Without the westward propagating wave signals, the weakening of

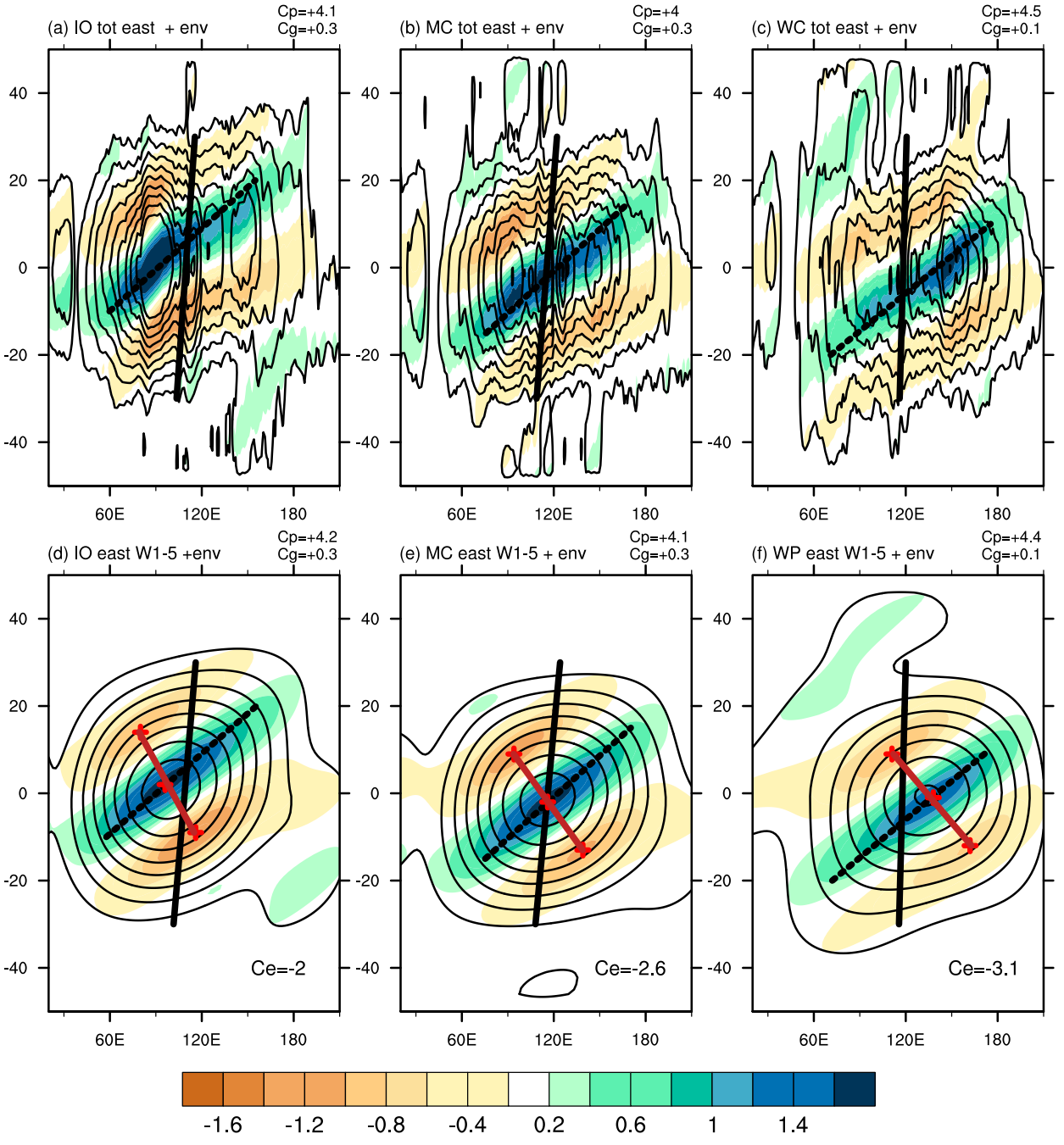

FIG. 4. The filtering of the MJO signals on Fig. 3 into (a)–(c) the total intraseasonal eastward propagating signals (mm; shadings) and (d)–(f) the intraseasonal eastward propagating wavenumber-1–5 signals (mm; shadings). The contours show the corresponding wave envelopes. The contour interval is 0.2 mm. The black dashed lines are the least squares fit of the precipitation maxima. The black solid lines are the least squares fit of the centroid longitudes of the wave envelopes. The brown solid lines in (d)–(f) are the least squares fit of the local extrema marked by the red crosses. The phase speed C_p, the group velocity C_g, and the propagation speed of the local extrema C_e are given.

the MJO convection signals over the MC region is less significant. However, the MC barrier effect is still presented and there is no obvious westward propagation of the local convection extrema in the total eastward propagating wave signals. When the total eastward propagating signals are further truncated at wavenumbers 1–5 (third column), the local extrema show significant westward propagation. Comparing the second and third

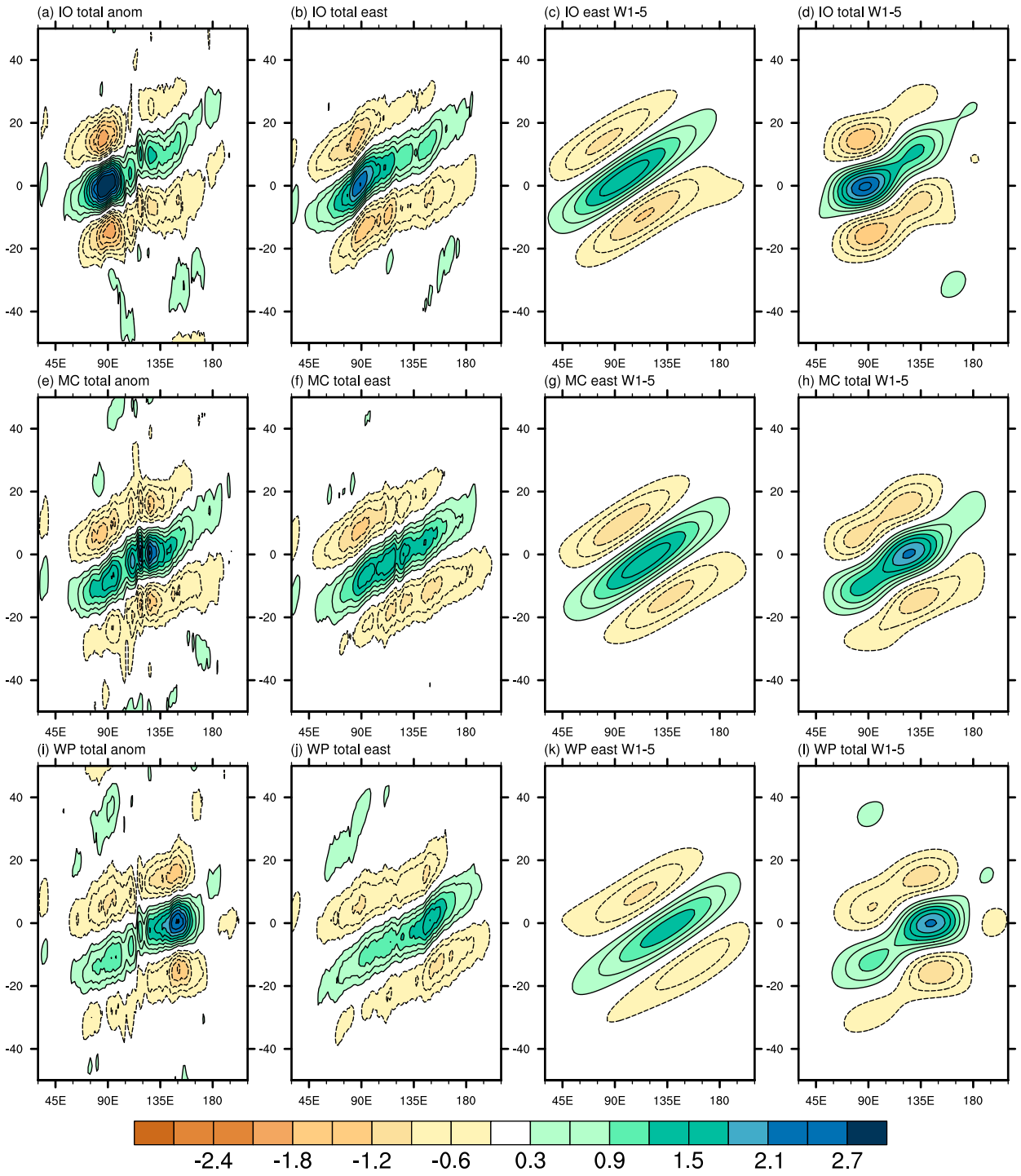

FIG. 5. Comparison of the MJO propagation features among different filtered MJO signals: (a),(e),(i) the total intraseasonal signals; (b), (f),(j) the total intraseasonal eastward propagating wave signals; (c),(g),(k) the intraseasonal eastward propagating wavenumber-1–5 signals; and (d),(h),(l) the total (eastward + westward) intraseasonal wavenumber-1–5 signals. The first column is identical to Fig. 3. The second to fourth columns are obtained by applying different filters to the first column.

columns indicates that the further truncation of the eastward propagating wave signals onto the planetary scales leads to the failure in resolving the MC barrier effect, which is reflected in the shifts of locations of the local convection extrema. These shifts of the local extrema cause artificial westward propagation of the local extrema. When the westward wavenumber-1–5 signals are included (fourth column), the MC barrier effect can be represented and there are no obvious westward propagations of the local convection extrema. Thus, it indicates that the westward propagation of local convection extrema is caused by the truncation of the MJO signals onto the planetary scales of the eastward propagating wavenumber domain. This truncation causes failure in representing the MC barrier effect, which is reflected in the shifts of the local convection extrema and a consequent significant westward propagation of the local convection extrema.

5. Conclusions

Using the TRMM precipitation datasets, it is shown that the MJO has a negligibly small group velocity during the northern winter (NDJFMA), which is supported by the quasi-constant frequency on the wavenumber–frequency spectra diagram and the nearly nonpropagating MJO wave envelopes on the regressed Hovmöller diagram. Using other datasets (e.g., daily outgoing longwave radiation data) or analyzing all-season range of the dataset will reveal the same conclusions (not shown here). The result of this study thus supports the idea that $\partial\omega/\partial k \approx 0$ should be considered as a target for the validation of MJO theories, as proposed by Majda and Stechmann (2009).

The discrepancy between the recent study (AK16) and our study is caused by the calculating method and the data filtering process. By definition, the group velocity is determined by the propagation of wave envelopes. However, the group velocity in AK16 is calculated by the propagation of the local convection extrema on the Hovmöller diagram, which does not necessarily indicate the propagation of the wave envelopes. More importantly, the Hovmöller diagram in AK16 was constructed by using only the eastward propagating zonal wavenumber-1–5 signals. The so-called MC barrier effect causes weak MJO convection amplitudes over the MC and strong amplitudes over the IO and the WP. When the MJO signals are truncated at the eastward propagating wavenumber-1–5 domain, they cannot represent this MC barrier effect. This causes the shifts of locations of the local convection extrema, which leads to significant westward propagation of the local convection extrema. When the total intraseasonal signals, or the total intraseasonal eastward propagating wave signals, or the total (eastward + westward) intraseasonal wavenumber-1–5 signals are used, the MC barrier effect can be represented and there are no obvious westward propagations of the local convection extrema. This indicates that the westward propagation of the local convection extrema is an artifact of the data filtering.

In the present study, we have shown that the MJO has a near-zero group velocity. However, the causes of this near-zero group velocity are complex. There are some linear theoretical models that can produce this near-zero group velocity (Majda and Stechmann 2009; Liu and Wang 2012, 2017a,b), while there are other models that produce westward group velocity (Adames and Kim 2016; Fuchs and Raymond 2017). Such divergent results are potentially due to the different simplifications made and different physical processes and parameterizations adopted in these models. Since the interaction among equatorial waves, convection, and moisture is important for the MJO and the MJO is regulated by the underlying SST distribution (Wang et al. 2016), the physical mechanism of the MJO dispersion relation is much more complicated than the theoretical dry tropical waves. Even for those linear models that capture, to some extent, the observed MJO dispersion relation, the underlying mechanisms are still unclear. Meanwhile, understanding the cause of the MJO dispersion relation and the associated near-zero group velocity may improve our understanding of the MJO propagation. Thus, more theoretical work is needed to find out the cause of near-zero group velocity for the MJO.

Acknowledgments. This work has been supported by the NSF Award AGS-1540783 and the Atmosphere–Ocean Research Center sponsored by the Nanjing University of Information Science and Technology and University of Hawaii. This is the SEOST Publication Number 10301, IPRC Publication Number 1309, and ESMC Publication Number 204.

REFERENCES

Adames, Á. F., and D. Kim, 2016: The MJO as a dispersive, convectively coupled moisture wave: Theory and observations. *J. Atmos. Sci.*, **73**, 913–941, https://doi.org/10.1175/JAS-D-15-0170.1.

Chen, G., and B. Wang, 2017: Reexamination of the wave activity envelope convective scheme in theoretical modeling of MJO. *J. Climate*, **30**, 1127–1138, https://doi.org/10.1175/JCLI-D-16-0325.1.

Duchon, C. E., 1979: Lanczos filtering in one and two dimensions. *J. Appl. Meteor.*, **18**, 1016–1022, https://doi.org/10.1175/1520-0450(1979)018<1016:LFIOAT>2.0.CO;2.

Fuchs, Ž., and D. J. Raymond, 2017: A simple model of intraseasonal oscillations. *J. Adv. Model. Earth Syst.*, **9**, 1195–1211, https://doi.org/10.1002/2017MS000963.

Hayashi, Y., 1971: A generalized method of resolving disturbances into progressive and retrogressive waves by space Fourier and time cross-spectral analyses. *J. Meteor. Soc. Japan*, **49**, 125–128, https://doi.org/10.2151/jmsj1965.49.2_125.

——, 1982: Space-time spectral analysis and its applications to atmospheric waves. *J. Meteor. Soc. Japan*, **60**, 156–171, https://doi.org/10.2151/jmsj1965.60.1_156.

Hendon, H. H., and M. C. Wheeler, 2008: Some space–time spectral analyses of tropical convection and planetary-scale waves. *J. Atmos. Sci.*, **65**, 2936–2948, https://doi.org/10.1175/2008JAS2675.1.

Huffman, G. J., and Coauthors, 2007: The TRMM Multisatellite Precipitation Analysis (TMPA): Quasi-global, multiyear, combined-sensor precipitation estimates at fine scales. *J. Hydrometeor.*, **8**, 38–55, https://doi.org/10.1175/JHM560.1.

Jiang, X., and Coauthors, 2015: Vertical structure and physical processes of the Madden–Julian oscillation: Exploring key model physics in climate simulations. *J. Geophys. Res. Atmos.*, **120**, 4718–4748, https://doi.org/10.1002/2014JD022375.

Knutson, T. R., K. M. Weickmann, and J. E. Kutzbach, 1986: Global-scale intraseasonal oscillations of outgoing longwave radiation and 250-mb zonal wind during Northern Hemisphere summer. *Mon. Wea. Rev.*, **114**, 605–623, https://doi.org/10.1175/1520-0493(1986)114<0605:GSIOOO>2.0.CO;2.

Liu, F., and B. Wang, 2012: A frictional skeleton model for the Madden–Julian oscillation. *J. Atmos. Sci.*, **69**, 2749–2758, https://doi.org/10.1175/JAS-D-12-020.1.

——, and ——, 2017a: Effects of moisture feedback in a frictional coupled Kelvin–Rossby wave model and implication in the Madden–Julian oscillation dynamics. *Climate Dyn.*, **48**, 513–522, https://doi.org/10.1007/s00382-016-3090-y.

——, and ——, 2017b: Roles of the moisture and wave feedbacks in shaping the Madden–Julian oscillation. *J. Climate.*, **30**, 10 275–10 291, https://doi.org/10.1175/JCLI-D-17-0003.1.

Madden, R. A., and P. R. Julian, 1971: Detection of a 40–50 day oscillation in the zonal wind in the tropical Pacific. *J. Atmos. Sci.*, **28**, 702–708, https://doi.org/10.1175/1520-0469(1971)028<0702:DOADOI>2.0.CO;2.

——, and ——, 1972: Description of global-scale circulation cells in the tropics with a 40–50 day period. *J. Atmos. Sci.*, **29**, 1109–1123, https://doi.org/10.1175/1520-0469(1972)029<1109:DOGSCC>2.0.CO;2.

Majda, A. J., and S. N. Stechmann, 2009: The skeleton of tropical intraseasonal oscillations. *Proc. Natl. Acad. Sci. USA*, **106**, 8417–8422, https://doi.org/10.1073/pnas.0903367106.

Persson, A., 2017: The story of the Hovmöller diagram: An (almost) eyewitness account. *Bull. Amer. Meteor. Soc.*, **98**, 949–957, https://doi.org/10.1175/BAMS-D-15-00234.1.

Roundy, P. E., and W. M. Frank, 2004: A climatology of waves in the equatorial region. *J. Atmos. Sci.*, **61**, 2105–2132, https://doi.org/10.1175/1520-0469(2004)061<2105:ACOWIT>2.0.CO;2.

Rui, H., and B. Wang, 1990: Development characteristics and dynamic structure of tropical intraseasonal convection anomalies. *J. Atmos. Sci.*, **47**, 357–379, https://doi.org/10.1175/1520-0469(1990)047<0357:DCADSO>2.0.CO;2.

Salby, M. L., R. R. Garcia, and H. H. Hendon, 1994: Planetary-scale circulations in the presence of climatological and wave-induced heating. *J. Atmos. Sci.*, **51**, 2344–2367, https://doi.org/10.1175/1520-0469(1994)051<2344:PSCITP>2.0.CO;2.

Wang, B., and S.-S. Lee, 2017: MJO propagation shaped by zonal asymmetric structures: Results from 24 GCM simulations. *J. Climate*, **30**, 7933–7952, https://doi.org/10.1175/JCLI-D-16-0873.1.

——, F. Liu, and G. Chen, 2016: A trio-interaction theory for Madden–Julian oscillation. *Geosci. Lett.*, **3**, 34, https://doi.org/10.1186/s40562-016-0066-z.

Wang, L., T. Li, E. Maloney, and B. Wang, 2017: Fundamental causes of propagating and nonpropagating MJOs in MJOTF/GASS models. *J. Climate*, **30**, 3743–3769, https://doi.org/10.1175/JCLI-D-16-0765.1.

Wheeler, M., and G. N. Kiladis, 1999: Convectively coupled equatorial waves: Analysis of clouds and temperature in the wavenumber–frequency domain. *J. Atmos. Sci.*, **56**, 374–399, https://doi.org/10.1175/1520-0469(1999)056<0374:CCEWAO>2.0.CO;2.

Zhang, C., 2005: Madden–Julian Oscillation. *Rev. Geophys.*, **43**, RG2003, https://doi.org/10.1029/2004RG000158.

——, 2013: Madden–Julian oscillation: Bridging weather and climate. *Bull. Amer. Meteor. Soc.*, **94**, 1849–1870, https://doi.org/10.1175/BAMS-D-12-00026.1.

——, and H. H. Hendon, 1997: Propagating and standing components of the intraseasonal oscillation in tropical convection. *J. Atmos. Sci.*, **54**, 741–752, https://doi.org/10.1175/1520-0469(1997)054<0741:PASCOT>2.0.CO;2.

——, and J. Ling, 2017: Barrier effect of the Indo-Pacific Maritime Continent on the MJO: Perspectives from tracking MJO precipitation. *J. Climate*, **30**, 3439–3459, https://doi.org/10.1175/JCLI-D-16-0614.1.